Strong tough hydrogels via the synergy of freeze-casting and salting out

https://doi.org/10.1038/s41586-021-03212-z

Received: 24 May 2020

Accepted: 8 January 2021

Published online: 24 February 2021

Check for updates

Mutian Hua[1,4], Shuwang Wu[1,2,4], Yanfei Ma[1], Yusen Zhao[1], Zilin Chen[1], Imri Frenkel[1], Joseph Strzalka[3], Hua Zhou[3], Xinyuan Zhu[2] & Ximin He[1]✉

Natural load-bearing materials such as tendons have a high water content of about 70 per cent but are still strong and tough, even when used for over one million cycles per year, owing to the hierarchical assembly of anisotropic structures across multiple length scales[1]. Synthetic hydrogels have been created using methods such as electro-spinning[2], extrusion[3], compositing[4,5], freeze-casting[6,7], self-assembly[8] and mechanical stretching[9,10] for improved mechanical performance. However, in contrast to tendons, many hydrogels with the same high water content do not show high strength, toughness or fatigue resistance. Here we present a strategy to produce a multi-length-scale hierarchical hydrogel architecture using a freezing-assisted salting-out treatment. The produced poly(vinyl alcohol) hydrogels are highly anisotropic, comprising micrometre-scale honeycomb-like pore walls, which in turn comprise interconnected nanofibril meshes. These hydrogels have a water content of 70–95 per cent and properties that compare favourably to those of other tough hydrogels and even natural tendons; for example, an ultimate stress of 23.5 ± 2.7 megapascals, strain levels of 2,900 ± 450 per cent, toughness of 210 ± 13 megajoules per cubic metre, fracture energy of 170 ± 8 kilojoules per square metre and a fatigue threshold of 10.5 ± 1.3 kilojoules per square metre. The presented strategy is generalizable to other polymers, and could expand the applicability of structural hydrogels to conditions involving more demanding mechanical loading.

Wood is light and strong; nacres are hard and resilient; muscles and tendons are soft and tough. These natural materials show a combination of normally contradicting mechanical properties, which is attributed to their hierarchical structures across multiple length scales[11]. Compared with natural load-bearing materials, conventional hydrogels with loose crosslinking, low solid content and homogeneous structure are relatively weak and fragile for handling real-world applications, which often demand long service periods, high load or impact tolerance, and large deformation. Tremendous improvements have been made to strengthen and toughen hydrogels by introducing mechanisms for energy dissipation during loading, such as by forming a double network[12,13], having dual crosslinking[14,15], self-assembly[8], inducing hydrophobic aggregation[16] and creating nano-crystalline domains[17,18]. These methods primarily focus on composition and molecular engineering, involving limited structural changes within a narrow length scale (molecular or nanoscale) and relatively simple structures compared to their complex structured natural counterparts.

Other advances take structural engineering approaches by creating anisotropic structures in hydrogels through freeze-casting[6,7], mechanical stretching[9,10,18,19] and compositing[4,5]. For example, directional freezing, or ice-templating, is widely used owing to its generic applicability to various polymers[7]. However, ice-templated hydrogels with micro-alignment have shown mechanical performance comparable to, or lower than, that of homogeneous tough hydrogels made by molecular engineering methods. Mechanical stretching has also been used to create anisotropic micro/nanostructures[9,10,18,19]. Alternatively, instead of in situ creating anisotropic structures within the hydrogel by ice-templating and mechanical stretching, compositing methods by addition of alien micro/nanoscale fibre reinforcements into hydrogel has also been explored[5,20–22]. The mechanically trained hydrogels and hydrogel composites have considerably improved strength and fracture toughness over homogeneous tough hydrogels, but also have limited stretchability or water content. These structural engineering approaches focus on optimizing the micro/nanostructures of existing hydrogels, yet it remains challenging to create simultaneously strong, tough, stretchable and fatigue-resistant hydrogels with more elaborate hierarchical structures across broader length scales, such as those observed in natural materials[23,24], while using a generic and facile approach.

Recently, an anisotropic composite of modulus-contrasting fibres and a matrix of similar composition has shown effectiveness for maintaining stretchability while improving strength, fracture toughness and fatigue resistance[4,25]. Therefore, forming a hierarchically anisotropic single-composition hydrogel containing strong and stretchable fibres of the same composition would be promising for making water-laden

[1]Department of Materials Science and Engineering, University of California, Los Angeles, Los Angeles, CA, USA. [2]School of Chemistry and Chemical Engineering, State Key Laboratory of Metal Matrix Composites, Shanghai Jiao Tong University, Shanghai, China. [3]X-Ray Science Division, Argonne National Laboratory, Lemont, IL, USA. [4]These authors contributed equally: Mutian Hua, Shuwang Wu. ✉e-mail: ximinhe@ucla.edu

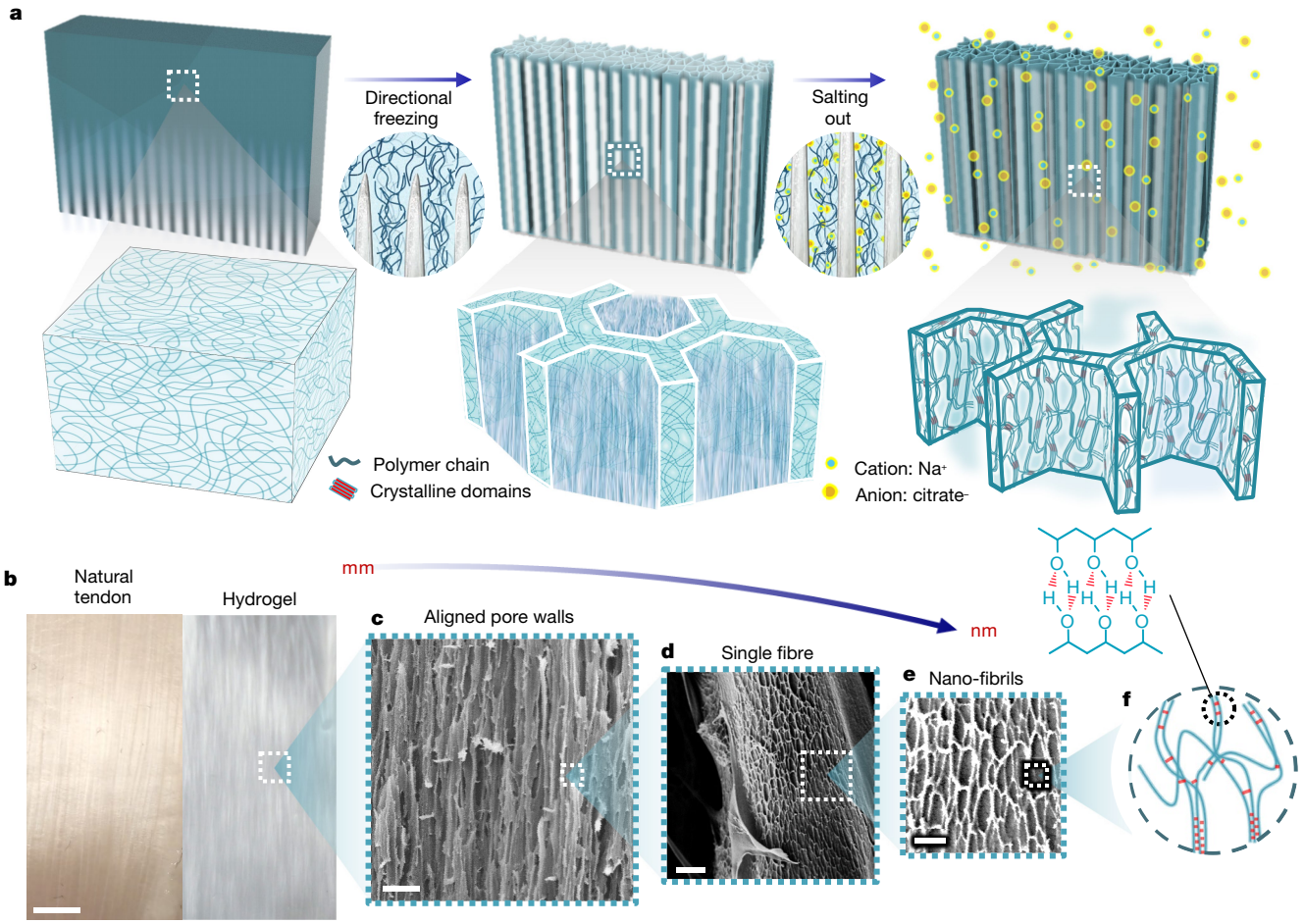

Fig. 1 | Fabrication and hierarchical structures of HA-PVA hydrogels. **a**, Freezing-assisted salting-out fabrication procedure of the HA-PVA hydrogels. Structural formation and polymer chain concentration, assembly and aggregation during the freezing-assisted salting-out fabrication process. **b**, Macroscopic view of real tendon and of the HA-5PVA hydrogel. Scale bar, 5 mm. **c**–**e**, SEM images showing the microstructure (**c**) and nanostructure (**d**, **e**) of the HA-5PVA hydrogel. Scale bars, 50 µm (**c**); 1 µm (**d**); 500 nm (**e**). **f**, Molecular illustration of polymer chains aggregated into nanofibrils.

hydrogels with simultaneously high strength, toughness, stretchability and fatigue threshold.

The alteration of polymer aggregation states could be realized by the simple addition of specific ions[26]; this is known as the Hofmeister effect[27], in which different ions have distinct abilities to precipitate polymers. With the aid of specific ions, modulus-contrasting structures could be formed from the same polymer composition. Meanwhile, directional freezing could endow hydrogels with anisotropic structures at the larger (micrometre–millimetre) scales while promoting molecular concentration. Herein, we propose to make hydrogels using a combination of molecular and structural engineering approaches. By combining directional freeze-casting and a subsequent salting-out treatment, which synergistically create hydrogel structures on different length scales across the millimetre scale to the molecular level (Fig. 1), we have constructed strong, tough, stretchable and fatigue-resistant hydrogels with hierarchical and anisotropic structures (denoted as HA-PVA/gelatin/alginate hydrogels).

Formation of hierarchical structures

Using poly(vinyl alcohol) (PVA) as a model system, a PVA solution was first directionally frozen and then directly immersed in a kosmotropic salt solution (Fig. 1a). A honeycomb-like micro-network with aligned pore walls was created during the directional freezing process (Fig. 1a, b)[6,7]. Importantly, the concentration and closer packing of polymer during freezing prepared the polymer chains for subsequent strong aggregation and crystallization induced by salting out. For the choice of kosmotropic ions we tested various species, obtaining a broad tunable range of gel microstructures and mechanical properties. Of those, sodium citrate showed the best salting-out ability and produced PVA hydrogel with the highest modulus (Supplementary Fig. 3). Under the influence of kosmotropic ions, the preconcentrated PVA chains strongly self-coalesced and phase-separated from the original homogeneous phase, which in turn formed the mesh-like nanofibril network on the surface of the micrometre-scale aligned pore walls[28] (Fig. 1d–f). The phase separation of PVA evolved over time until the elaborate structure and crystallinity developed and matured (Fig. 2c–e, Supplementary Fig. 4), and the non-phase-separated portion of PVA remained in between the nanofibrils as a continuous membrane that filled the nanofibril network (Fig. 1e).

Mechanistically, directional freezing concentrated PVA to form the aligned pore walls and increased the local concentration of PVA to higher values than the nominal concentration, whereas salting out strongly induced the aggregation and crystallization of PVA by phase separation to form the nanofibrils. To understand the synergistic effects of freezing and salting out in this combined method, we designed a series of gel preparation methods with one or several factors omitted for direct comparisons (Fig. 3, Extended Data Fig. 1). As control samples, the PVA hydrogels prepared by directional freezing alone (Fig. 3c, Extended Data Fig. 2a) or salting out alone (Extended Data Fig. 1f, Extended Data Fig. 2b) showed strength, toughness and stretchability that were all lower than those of HA-PVA hydrogels (Fig. 3a,

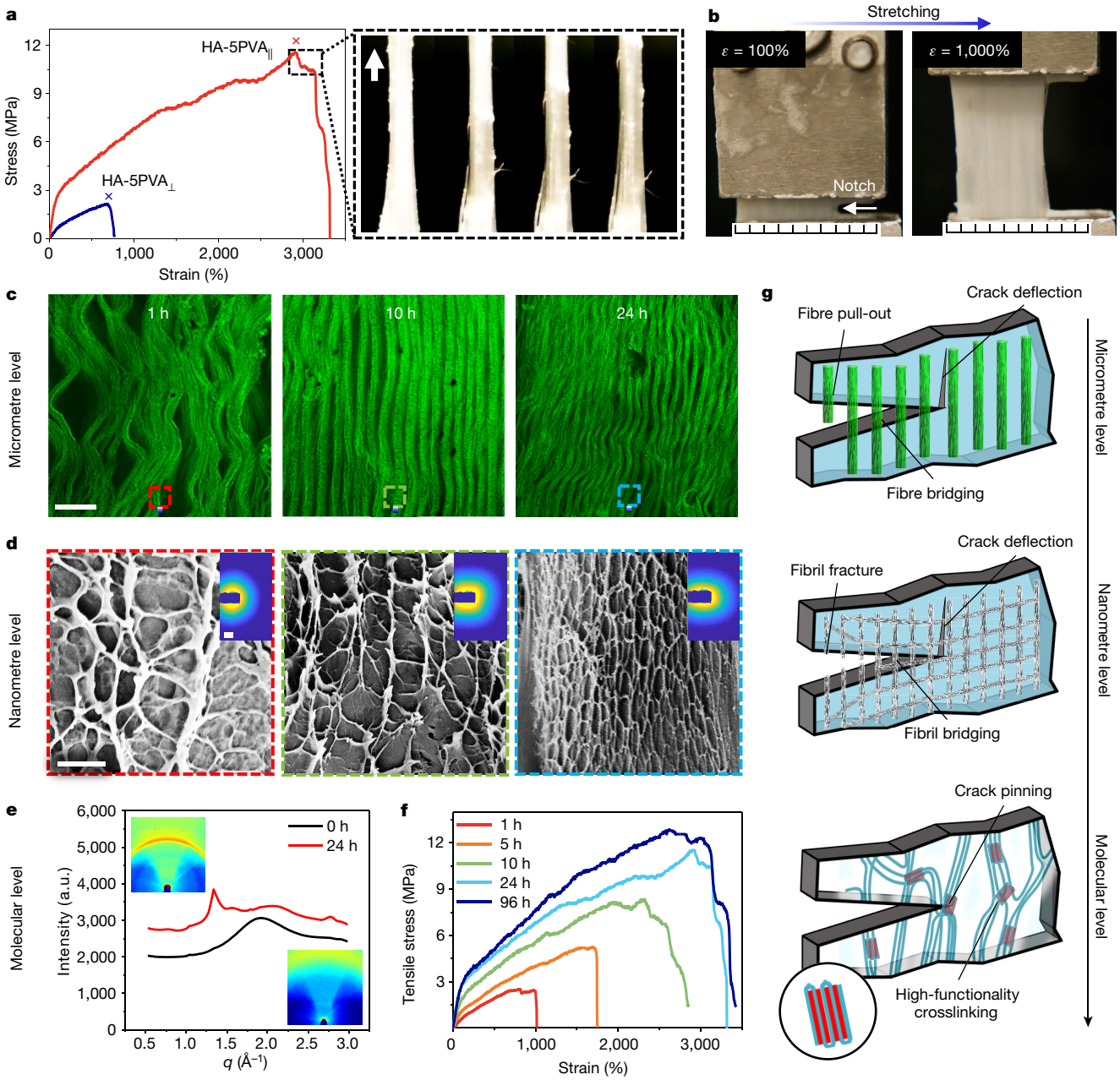

Fig. 2 | Mechanical properties and structural evolution of HA-PVA hydrogel. a, Tensile stress–strain curve of HA-5PVA hydrogel in the parallel (∥) and perpendicular (⊥) directions relative to the alignment direction. The image on the right shows the fibrotic fracture of the HA-5PVA$_{\parallel}$ hydrogel. **b**, Tensile loading of a HA-5PVA$_{\parallel}$ hydrogel with a pre-made crack. ε, strain. **c**, Confocal images showing the microstructures of HA-5PVA$_{\parallel}$ hydrogels after different periods of salting out in 1.5 M sodium citrate. Scale bar, 50 µm. **d**, SEM images showing the evolution of the nanofibril network within the microstructure during the salting-out process. Scale bar, 5 µm. The insets show the corresponding SAXS patterns of freeze-dried HA-5PVA$_{\parallel}$ hydrogel; scale bar, 0.01 Å^{-1}. **e**, Wide-angle X-ray scattering (WAXS) patterns of HA-5PVA$_{\parallel}$ hydrogel (top) compared with a PVA hydrogel of the same polymer content prepared by repeated freeze–thaw cycles (bottom) and the corresponding integrated scattering intensity with scattering vector **q** with q = 0.5–3 Å^{-1}. The peak at q = 1.35 Å^{-1} corresponds to the crystalline peak around a diffraction angle of 2Θ = 18° obtained using 8-keV X-ray diffraction. Scale bar, 0.5 Å^{-1}; a.u., arbitrary units. **f**, Stress–strain curve of HA-5PVA$_{\parallel}$ hydrogels after different periods of salting out in 1.5 M sodium citrate. **g**, Toughening mechanisms at each length scale.

Extended Data Fig. 2). Structure-wise, the directionally frozen PVA hydrogel without the subsequent salting out showed only aligned pore walls, without the mesh-like nanofibrils (Fig. 3c, Supplementary Fig. 5), which suggested weak aggregation of polymer chains in the absence of salting-out treatment. On the other hand, directly salting out the PVA without prior freezing did not yield a bulk hydrogel, and instead formed loosely and randomly entangled fibrils (Extended Data Fig. 1f), which suggested that pre-freezing the PVA solution provided the necessary confinement and preconcentration of PVA chains for effective phase separation during the subsequent salting out to form a strong bulk material. In short, such a freezing-assisted salting-out method presents a unique synergy that seamlessly integrates the advantages of the two techniques to boost the effect of aggregation, and is crucial for achieving simultaneously high strength, toughness, stretchability and structural hierarchy in the HA-PVA hydrogels.

Strengthening while toughening

The HA-PVA hydrogels showed distinct mechanical properties in the parallel and perpendicular direction relative to the alignment direction

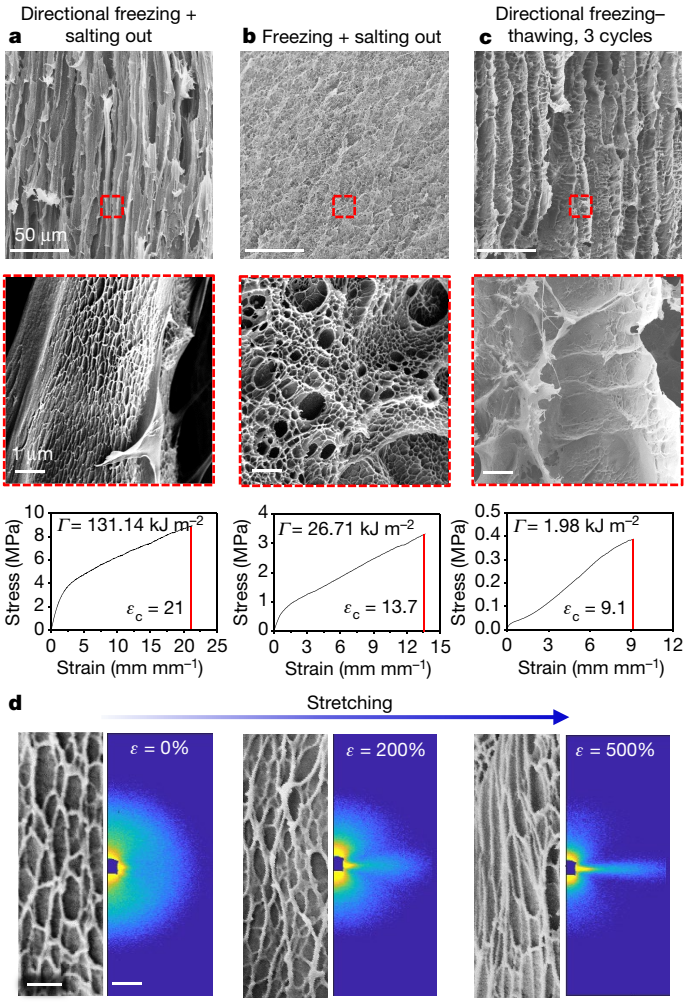

Fig. 3 | Hydrogel structure and mechanical properties relationship. **a**–**c**, SEM images and mechanical properties of HA-5PVA hydrogel prepared by directional freezing and subsequent salting out (**a**), 5PVA hydrogel prepared by uniform freezing and subsequent salting out (**b**; non-directional, in contrast to **a**) and 5PVA hydrogel prepared by directional freezing and thawing for three cycles (**c**; no salting out, unlike **a**). Scale bars, 50 μm (top row), 1 μm (middle row, zoomed-in SEM images). **d**, SEM images (left) showing the deformation of the mesh-like nanofibril network during stretching and corresponding in situ SAXS patterns (right). Scale bars, 1 μm (SEM images); 0.025 $Å^{-1}$ (SAXS images).

owing to the induced anisotropy (denoted as HA-*x*PVA for *x*% PVA precursor). Notably, the HA-5PVA hydrogels demonstrated superior toughness of 175 ± 9 MJ m^{-3} upon stretching in the direction parallel to the alignment, with an ultrahigh ultimate stress of 11.5 ± 1.4 MPa and ultimate strain of 2,900 ± 450% after 24 h of salting out (Fig. 2a). Even when stretched in the relatively weaker perpendicular direction, the HA-5PVA hydrogel was as tough as previously reported tough hydrogels[14,16]. The HA-5PVA hydrogel showed a gradual failure mode featuring stepwise fracture and pull-out of fibres, which are typical for highly anisotropic materials (Fig. 2a, right). There was no observable crack propagation perpendicular to the stretch direction during tensile loading of the hydrogel (Supplementary Video 1). Even with pre-existing cracks, the hydrogel showed a remarkable crack-blunting ability, and the initial crack did not advance into the material at high strains, indicating flaw-insensitivity[18] (Fig. 2b, Supplementary Video 2).

The unusual combination of high strength and high toughness was correlated with three structural aspects at the micrometre, nanometre and molecular levels that evolved during synthesis (Fig. 2c–e), which integrated multiple strengthening and toughening mechanisms. For instance, the densification of aligned micropore walls (Fig. 2c) and nanofibrils (Fig. 2d) strengthened the material by increasing the material density, and toughened it by increasing the energy dissipation during fracture. Additionally, the growing crystallinity during salting out (Fig. 2e, Supplementary Fig. 4; 40% crystallinity after 24 h) strengthened each nanofibril and improved material elasticity, owing to the crystalline domains acting as rigid, high-functionality crosslinkers[24], and toughened the fibrils by virtue of their ability to delay the fracture of individual fibrils by crack-pinning (Fig. 2g)[17]. In short, the strengthening mechanism was mainly structural densification due to hydrogen bonds and crystalline domains formation, and the toughening mechanisms were pull-out, bridging and energy dissipation by the fibrils (Fig. 2g, Supplementary Fig. 6). During the evolution of these structures across multiple length scales, the strength, stretchability and toughness of the HA-PVA hydrogel increased simultaneously (Fig. 2f).

Structure–property correlation

The three structural aspects at different length scales are intertwined in the present material. To identify their roles in the synergistic strengthening and toughening, we compared the mechanical performances (critical stress σ_c, critical strain ε_c and fracture energy Γ) of a series of PVA hydrogels with different combinations of those three structural aspects (Fig. 3a–c, Extended Data Fig. 1, Supplementary Fig. 7) with a conventional chemically crosslinked PVA hydrogel in which none of these structures existed (Extended Data Fig. 1e). Forming only low-density crystalline domains (Extended Data Fig. 1d) or aligned pore walls (Fig. 3c) by the conventional freeze–thaw method did not show remarkable enhancement in mechanical performance, whereas the formation of nanofibril networks (Fig. 3b) led to a nearly two-orders-of-magnitude increase in strength and a four-orders-of-magnitude increase in toughness compared to the baseline. The addition of anisotropic microstructure (via directional freezing) further enhanced the strength and toughness, but the increase was less pronounced (Fig. 3a). We conclude that among the multiple aforementioned mechanisms, which all have important roles, the effect of the nanofibril network was particularly prominent for simultaneous high strength, toughness and stretchability (Supplementary Information section 3).

The formed nanofibrils were not rigid, but rather stretchable, and deformed along with the hydrogel during stretching, as depicted in the scanning electron microscope (SEM) images of Fig. 3d. The nanofibrils became increasingly aligned after stretching, as indicated by the stretch of the small-angle X-ray scattering (SAXS) pattern perpendicular to the loading direction (Fig. 3d). The average nanofibril spacing decreased from about 350 nm to about 200 nm (Fig. 3d, Supplementary Fig. 8) when the strain increased from 0% to 500%. These stretchable nanofibrils strengthen and toughen the hydrogel, in a similar way to rigid-fibre reinforcements used in composite hydrogels, yet they are stretchable to preserve the stretchability of the hydrogel, which is key to achieving high strength, toughness and stretchability[4,25] simultaneously. From a fracture mechanics perspective (Supplementary Information section 4), first, the formation of a continuously connected network facilitates the stress transfer between individual fibrils and prevent inter-fibril sliding, and thus energy dissipation ahead of a crack tip is not confined to the vicinity of the crack tip but rather expands to the entire network (Supplementary Fig. 9). Equivalently, the connection of nanofibrils via a continuous network extends their length, and longer polymer fibres along the stress direction result in higher toughness[4]. Second, the fracture energy of amorphous hydrogel can be calculated as[24,29]

$$\Gamma \propto U_f N_f,$$

where U_f is the energy required to fracture a single polymer chain and N_f is the number of polymer chains fractured. Owing to the strong aggregation and crystalline domains in the nanofibrils, the energy required to

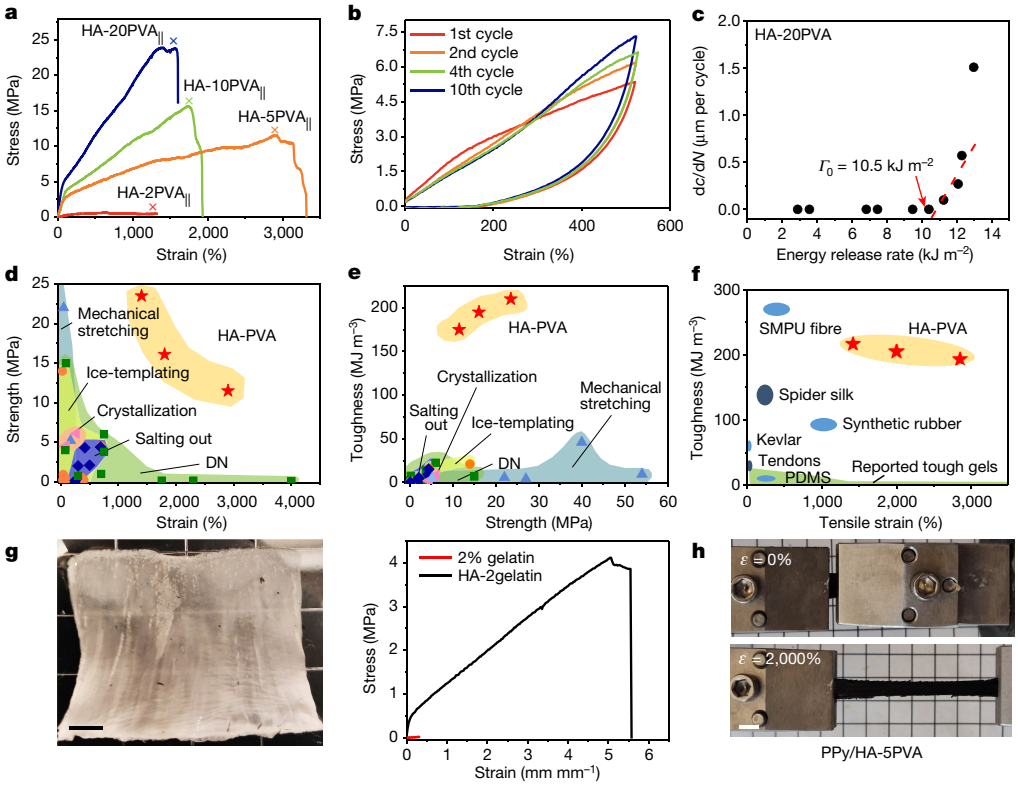

Fig. 4 | Tunable mechanical properties and generality of hydrogels produced by ice-templating-assisted salting out. a, Stress–strain curves of HA-2PVA$_{||}$, 5PVA$_{||}$, 10PVA$_{||}$ and 20PVA$_{||}$ hydrogels after 24 h of salting out in 1.5 M sodium citrate. **b**, Cyclic loading of HA-5PVA$_{||}$ hydrogel to 500% strain. **c**, Crack propagation per loading cycle, dc/dN, under increasing energy release rate. The energy release rate was controlled by the corresponding maximum strain. **d**–**f**, Ashby diagrams of ultimate tensile strength versus ultimate tensile strain (**d**), toughness versus ultimate tensile strength (**e**) and toughness versus ultimate tensile strain (**f**) of HA-PVA hydrogels, other reported tough hydrogels and other tough materials. The data used are summarized in Supplementary Table 3. **g**, Photograph of HA-2gelatin hydrogel prepared by the same method as HA-PVA (left) and stress–strain curves of HA-2gelatin and regular 2% gelatin hydrogel (right). Scale bar, 5 mm. **h**, PPy-infiltrated HA-5PVA$_{||}$ hydrogel being stretched. Scale bar, 5 mm. DN, double-network hydrogels; SMPU, shape-memory poly(urethane).

fracture the same number of crystalized polymer chains is much higher than that needed for non-packed amorphous chains[30]. The entire bulk hydrogel is a continuous micrometre-scale network comprising the above strong nanofibril networks, which largely account for its high strength, toughness and stretchability.

Tunability and fatigue resistance

We varied the densities of the aligned micropore walls and nanofibrils by changing the initial PVA concentration from 2% to 20%, and reached ultimate stresses of 23.5 ± 2.7 MPa, 16.1 ± 1.8 MPa and 11.5 ± 1.4 MPa and corresponding ultimate strains of 1,400 ± 210%, 1,800 ± 330% and 2,900 ± 450% after 24 h of salting out (Fig. 4a, Supplementary Fig. 10). For hydrogels with sufficient structural density and PVA concentration above 5%, the ultimate stress increased with PVA concentration, whereas the ultimate strain decreased with increasing PVA concentration, and the overall toughness increased with PVA concentration. The fracture energy ranged from 131 ± 6 kJ m^{-2} to 170 ± 8 kJ m^{-2} (Extended Data Fig. 4b) as the PVA concentration increased from 5 wt% to 20 wt%, as measured with a pre-cut crack perpendicular to the fibres. It should be noted that crack redirection was observed for the HA-5PVA and HA-10PVA hydrogels during the fracture energy measurements (Supplementary Fig. 11), and the substantial blunting of crack size makes these hydrogels flaw-insensitive[18]. Therefore, the measured fracture energy becomes related to the sample size. For the same sample size, the fracture energy of HA-5PVA was 5 and 65 times higher than those of the hydrogel with nanofibrils only (Fig. 3b, Supplementary Video 4) and the hydrogel with aligned porous microstructure only (Fig. 3c), respectively, where the measured fracture energy is the true material property.

We further studied the reversibility and reusability of the HA-PVA hydrogels by conducting multiple loading–unloading tests (Fig. 4b, Supplementary Fig. 12). Mechanical hysteresis was observed for all samples tested (Fig. 4b), which indicated the presence of sacrificial bonds (primarily hydrogen bonds here) that broke during deformation. The maximum stress increased with the number of stretching cycles owing to improved alignment induced by stretching[10,19]. The hysteresis area did not show obvious decrease over ten cycles, which indicated that the sacrificial hydrogen bonds responsible for energy dissipation were mostly reversible.

Fatigue resistance is another important criterion for structural hydrogels, and its limit is usually much lower than the fracture energy. To provide an accurate measurement, we used the relatively rigid HA-20PVA, in which crack redirection was less likely to occur (Supplementary Video 3, Supplementary Information section 5). The HA-20PVA hydrogels showed excellent fatigue resistance with a fatigue threshold of 10.5 ± 1.3 kJ m^{-2} (Fig. 4c, Extended Data Fig. 3), which is eight times higher than the highest reported value for existing tough hydrogels[17,19]. No crack propagation or redirection was observed for over 30,000 cycles with such a high energy release rate (Extended Data Fig. 3b). The highly fatigue-resistant HA-PVA hydrogels utilize the crystalline domains and networks of fibres as strong barriers to cracks such as those in tendons and other robust natural materials.

Overall, the HA-PVA hydrogels showed high ultimate stress and strain that well surpassed the values seen in many reported tough hydrogels (Fig. 4d), with an overall toughness increased by 4 to 10^3 times

(Fig. 4e). The HA-PVA hydrogels demonstrated excellent toughness of 175 ± 9 MJ m^{-3} to 210 ± 13 MJ m^{-3} in the absence of flaws, as the direct result of their combination of high strength and high ductility (Fig. 4e). At a water content of over 70% in these hydrogels (Extended Data Fig. 4a), these toughness values are well above those of water-free polymers such as polydimethylsiloxane (PDMS)[31], Kevlar and synthetic rubber[32], even surpassing the toughness of natural tendon[1] and spider silk[33] (Fig. 4f).

Generality and customizability

Using the freezing-assisted salting-out strategy, we also fabricated gelatin and alginate hydrogels with enhanced mechanical properties. Regular 2% gelatin hydrogels are weak and fragile, whereas the HA-2gelatin hydrogel could be stretched to 4 MPa and 550% strain, which led to an over 1,000-fold increase in toughness (from 0.0075 ± 0.0006 MJ m^{-3} to 11.9 ± 1.7 MJ m^{-3}) (Fig. 4g). Likewise, HA-5alginate, which is a pure alginate hydrogel without calcium crosslinking, showed an ultimate strength of 1.1 ± 0.2 MPa and an over-20-fold increase in toughness compared to calcium-crosslinked alginate hydrogel (Extended Data Fig. 5). Building upon the combination of high strength, stretchability and fatigue resistance of these HA-PVA hydrogels, we demonstrated the facile customizability of additional properties (for example, electrical conductivity) for their application in other fields. Here, by infiltrating the HA-PVA hydrogel with a conducting polymer (for example, poly-pyrrole; PPy), the hydrogel was functionalized to have electrical conductivity, without affecting its strength nor toughness (Fig. 4h, Supplementary Fig. 13).

Conclusion

In this study, we developed hierarchically structured hydrogels that combine high strength, toughness, stretchability and fatigue resistance, using a freezing-assisted salting-out treatment. Considering that the Hofmeister effect exists for various polymers and solvent systems, we are convinced that the presented strategy is not restricted to the systems presented here. We foresee that with the help of the presented strategy, originally weak hydrogels could be applied in the medical, robotics, energy and additive manufacturing fields.

Online content

Any methods, additional references, Nature Research reporting summaries, source data, extended data, supplementary information, acknowledgements, peer review information; details of author contributions and competing interests; and statements of data and code availability are available at https://doi.org/10.1038/s41586-021-03212-z.

1. Maganaris, C. N. & Paul, J. P. In vivo human tendon mechanical properties. *J. Physiol. (Lond.)* **521**, 307–313 (1999).
2. Gu, L., Jiang, Y. & Hu, J. Scalable spider-silk-like supertough fibers using a pseudoprotein polymer. *Adv. Mater.* **31**, 1904311 (2019).
3. Hong, S. et al. 3D printing of highly stretchable and tough hydrogels into complex, cellularized structures. *Adv. Mater.* **27**, 4034–4040 (2015).
4. Xiang, C. et al. Stretchable and fatigue-resistant materials. *Mater. Today* **34**, 7–16 (2020).
5. Huang, Y. et al. Energy-dissipative matrices enable synergistic toughening in fiber reinforced soft composites. *Adv. Funct. Mater.* **27**, 1605350 (2017).
6. Zhang, H. et al. Aligned two- and three-dimensional structures by directional freezing of polymers and nanoparticles. *Nat. Mater.* **4**, 787–793 (2005).
7. Zhang, H. *Ice Templating and Freeze-Drying for Porous Materials and their Applications* (Wiley-VCH, 2018).
8. Qin, H., Zhang, T., Li, N., Cong, H. P. & Yu, S. H. Anisotropic and self-healing hydrogels with multi-responsive actuating capability. *Nat. Commun.* **10**, 2202 (2019).
9. Mredha, M. T. I. et al. Anisotropic tough multilayer hydrogels with programmable orientation. *Mater. Horiz.* **6**, 1504–1511 (2019).
10. Mredha, M. T. I. et al. A facile method to fabricate anisotropic hydrogels with perfectly aligned hierarchical fibrous structures. *Adv. Mater.* **30**, 1704937 (2018).
11. Wegst, U. G. K., Bai, H., Saiz, E., Tomsia, A. P. & Ritchie, R. O. Bioinspired structural materials. *Nat. Mater.* **14**, 23–36 (2015).
12. Sun, J.-Y. et al. Highly stretchable and tough hydrogels. *Nature* **489**, 133–136 (2012).
13. Gong, J. P., Katsuyama, Y., Kurokawa, T. & Osada, Y. Double-network hydrogels with extremely high mechanical strength. *Adv. Mater.* **15**, 1155–1158 (2003).
14. Hu, X., Vatankhah-Varnoosfaderani, M., Zhou, J., Li, Q. & Sheiko, S. S. Weak hydrogen bonding enables hard, strong, tough, and elastic hydrogels. *Adv. Mater.* **27**, 6899–6905 (2015).
15. Lin, P., Ma, S., Wang, X. & Zhou, F. Molecularly engineered dual-crosslinked hydrogel with ultrahigh mechanical strength, toughness, and good self-recovery. *Adv. Mater.* **27**, 2054–2059 (2015).
16. He, Q., Huang, Y. & Wang, S. Hofmeister effect-assisted one step fabrication of ductile and strong gelatin hydrogels. *Adv. Funct. Mater.* **28**, 1705069 (2018).
17. Lin, S. et al. Anti-fatigue-fracture hydrogels. *Sci. Adv.* **5**, eaau8528 (2019).
18. Bai, R., Yang, J., Morelle, X. P. & Suo, Z. Flaw-insensitive hydrogels under static and cyclic loads. *Macromol. Rapid Commun.* **40**, 1800883 (2019).
19. Lin, S., Liu, J., Liu, X. & Zhao, X. Muscle-like fatigue-resistant hydrogels by mechanical training. *Proc. Natl Acad. Sci. USA* **116**, 10244–10249 (2019).
20. Illeperuma, W. R. K., Sun, J. Y., Suo, Z. & Vlassak, J. J. Fiber-reinforced tough hydrogels. *Extreme Mech. Lett.* **1**, 90–96 (2014).
21. Lin, S. et al. Design of stiff, tough and stretchy hydrogel composites via nanoscale hybrid crosslinking and macroscale fiber reinforcement. *Soft Matter* **10**, 7519–7527 (2014).
22. King, D. R., Okumura, T., Takahashi, R., Kurokawa, T. & Gong, J. P. Macroscale double networks: design criteria for optimizing strength and toughness. *ACS Appl. Mater. Interfaces* **11**, 35343–35353 (2019).
23. Fan, H. & Gong, J. P. Fabrication of bioinspired hydrogels: challenges and opportunities. *Macromolecules* **53**, 2769–2782 (2020).
24. Zhao, X. Multi-scale multi-mechanism design of tough hydrogels: building dissipation into stretchy networks. *Soft Matter* **10**, 672–687 (2014).
25. Wang, Z. et al. Stretchable materials of high toughness and low hysteresis. *Proc. Natl Acad. Sci. USA* **116**, 5967–5972 (2019).
26. Iwaseya, M., Watanabe, M., Yamaura, K., Dai, L. X. & Noguchi, H. High performance films obtained from PVA/Na_2SO_4/H_2O and PVA/CH_3COONa/H_2O systems. *J. Mater. Sci.* **40**, 5695–5698 (2005).
27. Zhang, Y. & Cremer, P. S. Interactions between macromolecules and ions: the Hofmeister series. *Curr. Opin. Chem. Biol.* **10**, 658–663 (2006).
28. van de Witte, P., Dijkstra, P. J., Van Den Berg, J. W. A. & Feijen, J. Phase separation processes in polymer solutions in relation to membrane formation. *J. Membr. Sci.* **117**, 1–31 (1996).
29. Lake, G. J. & Thomas, A.G. The strength of highly elastic materials. *Proc. R. Soc. A* **300**, 108–119 (1967).
30. Kinloch, A. J. & Young, R. J. (eds) *Fracture Behaviour of Polymers* (Springer Science & Business Media, 1984).
31. Johnston, I. D., McCluskey, D. K., Tan, C. K. L. & Tracey, M. C. Mechanical characterization of bulk Sylgard 184 for microfluidics and microengineering. *J. Micromech. Microeng.* **24**, 035017 (2014).
32. Wood, L. A. Uniaxial extension and compression in stress-strain relations of rubber. *Rubber Chem. Technol.* **51**, 840–851 (1978).
33. Ebrahimi, D. et al. Silk – its mysteries, how it is made, and how it is used. *ACS Biomater. Sci. Eng.* **1**, 864–876 (2015).

Methods

Preparation of PVA solution

2 wt%, 5 wt%, 10 wt% and 20 wt% PVA solutions were prepared by dissolving PVA powder in deionized water under vigorous stirring and heating (70 °C). After degassing by sonication for 1 h, a clear solution was obtained.

Preparation of salt solution

A 1.5 M sodium citrate solution was prepared by dissolving anhydrous sodium citrate powder in deionized water. After sonication for 10 min, a clear solution was obtained.

Fabrication of hydrogel

An ethanol bath at −80 °C was used as the immersion bath for ice-templating. The temperature was maintained using an EYELA-PSL1810 constant-temperature bath. For a typical fabrication of the hierarchically aligned PVA hydrogels, 2–20% PVA aqueous precursor is poured into an acrylic container with peripheral thermal insulation and a glass bottom for good thermal conduction. The container is lowered into the ethanol bath at an immersion rate of 1 mm min^{-1}. The directionally frozen PVA solution is then immersed into a 1.5 M sodium salt solution for gelation for up to 4 days.

Tensile testing

The hydrogels were cut into dog-bone-shaped specimens with a gauge width of 2 mm for regular tensile testing. The thickness of the individual specimens was measured with a calliper and was typically around 2 mm. The HA-xPVA$_{\parallel}$ specimens had a microstructure parallel to the loading direction and the HA-xPVA$_{\perp}$ specimens had a microstructure perpendicular to the loading direction. The force–displacement data were obtained using a Cellscale Univert mechanical tester equipped with 50-N and 200-N loading cells. The stress–strain curves were obtained by dividing the measured force by the initial gauge cross-section area and dividing the measured displacement by the initial clamp distance. Five hydrogel specimens were tested for each condition.

Pure shear tests

The hydrogels were cut into rectangular specimens with a height of 40 mm and a width of 20 mm for the fracture tests. The thickness of individual specimens was measured with a calliper. An initial clamp distance of 1 mm or 2 mm was used for every pair of specimens. All specimens had microstructure alignment parallel to the height direction. For pure shear tests, two identical samples (one notched, one unnotched) were loaded under the sample setup as a pair to obtain one fracture energy value[12]. Briefly, for the notched samples, an initial 8-mm-long straight cut was made from the middle of the long edge towards the centre of the hydrogel, and the specimen was loaded at a strain rate of 10% s^{-1}. The critical strain (ε_c) for unstable propagation of the crack was obtained from the strain at maximum stress. The pairing unnotched specimens were subsequently loaded until $\varepsilon = \varepsilon_c$. The fracture energy value was obtained by multiplying the area under the stress–strain curve of the unnotched specimens with the initial clamp distance (H) as $\Gamma = H\int_0^{\varepsilon_c} \sigma \mathrm{d}\varepsilon$.

Fatigue tests

To examine the fatigue resistance of our hydrogel, we adopted the single-notch method[34]. Fatigue testing was performed in a water bath to prevent dehydration of the hydrogel. Cyclic tensile tests were conducted using notched samples with initial crack length (c_0) smaller than 1/5 of the width (L_0) of the sample. The sample width L_0 was much smaller than the sample height H_0. The cyclic force–displacement curves were obtained using a Cellscale Univert mechanical tester. A digital camera was used to monitor the crack propagation of the hydrogel. All stretch cycles were conducted continuously without a relaxation time. The energy release rate (G) was obtained using

$$G = 2kcW,$$

where k is a function that varies with strain, which was empirically determined to be $k = 3/\sqrt{\varepsilon + 1}$, c is the crack length and W is the strain energy density of an unnotched sample with the same dimensions and stretched to the same strain ε. It should be noted that when repeatedly stretching to high strains, the stress–strain curve slowly deviates from the initial loading–unloading curve as a result of plastic deformation, and W is integrated from the loading part, where the loading–unloading curves become stable.

SEM characterization

For characterization of the micro- and nanostructure of the hierarchically aligned hydrogels, all hydrogel samples were immersed in deionized water for 24 h before freeze-drying using a Labconco FreeZone freeze-dryer. The freeze-dried hydrogels were cut along the aligned direction to expose their interior and sputtered with gold before carrying out imaging using a ZEISS Supra 40VP SEM.

Confocal characterization

Confocal microscopy was carried out using a Leica DMi8 confocal microscope. 0.1 wt% fluorescein sodium salt was added to the PVA precursor as a fluorescent marker, and florescent HA-PVA hydrogels were made with the same fabrication procedures as regular HA-PVA hydrogels. The 488-nm laser channel was used to excite the fluorescent marker. The hydrogel was assigned a green pseudo-colour.

X-ray scattering characterization

The HA-PVA hydrogels were cut into 1 × 4 cm^2 rectangles and washed with deionized water before testing. The beamline station used was APS 8-ID-E (Argonne National Laboratory), which is equipped with the Pilatus 1M detector. A customized linear stretcher was used to hold the samples and stretch on demand for in situ X-ray scattering measurements. The MATLAB toolbox GIXSGUI was used for further editing and analysis of the scattering patterns[35].

Water content measurement

We measured the water content of the HA-PVA hydrogels by comparing their weights before and after freeze-drying. Excess surface water was wiped from the hydrogel surface and the hydrogel specimens were instantly frozen using liquid nitrogen, followed by freeze-drying. The weight before (m_w) and after (m_d) freeze-drying was measured with a balance. The water content was obtained as $[(m_w - m_d)/m_w] \times 100\%$.

Crystallinity content measurement

Before freeze-drying the hydrogels for differential scanning calorimetry (DSC) measurements, we first used excess chemical crosslinks induced by glutaraldehyde to fix the amorphous PVA polymer chains in order to minimize further formation of crystalline domains during the drying process following ref. [19]. The water content of the hydrogel, f_{water}, was obtained by comparing the weight before and after freeze-drying. In a typical DSC measurement, we first measured the total mass of the freeze-dried sample, m. The sample was subsequently placed in a Tzero pan and heated up from 50 °C to 250 °C at a rate of 20 °C min^{-1} under a nitrogen atmosphere with a flow rate of 30 ml min^{-1}. The curve of the heat flow shows another narrow peak ranging from 200 °C to 250 °C, which corresponds to the melting of the crystalline domains. The integration of the endothermic transition from 200 °C to 250 °C gives the enthalpy for the melting of the crystalline domains per unit mass of the dry samples. Therefore, the mass of the crystalline domains $m_{crystalline}$ can be calculated as $m_{crystalline} = mH_{crystalline}/H^0_{crystalline}$ where $H^0_{crystalline} = 138.6$ J g^{-1} is the enthalpy of the fusion of 100 wt%

crystalline PVA measured at the equilibrium melting point, T_m^0 (ref. [36]). Therefore, the crystallinity in the dry sample, X_{dry}, can be calculated as $X_{dry} = m_{crystalline}/m$. With the measured water content from freeze-drying, the crystallinity in the swollen state can be calculated as $X_{swollen} = X_{dry}(1 - f_{water})$.

Data availability

The data that support the findings of this study are available from the corresponding author on reasonable request.

34. Long, R. & Hui, C. Y. Fracture toughness of hydrogels: measurement and interpretation. *Soft Matter* **12**, 8069–8086 (2016).
35. Jiang, Z. GIXSGUI: a MATLAB toolbox for grazing-incidence X-ray scattering data visualization and reduction, and indexing of buried three-dimensional periodic nanostructured films. *J. Appl. Cryst.* **48**, 917–926 (2015).
36. Peppas, N. A. & Merrill, E. W. Differential scanning calorimetry of crystallized PVA hydrogels. *J. Appl. Polym. Sci.* **20**, 1457–1465 (1976).

Acknowledgements This research was supported by NSF CAREER award 1724526, AFOSR awards FA9550-17-1-0311, FA9550-18-1-0449 and FA9550-20-1-0344, and ONR awards N000141712117 and N00014-18-1-2314. X.Z. acknowledges Shanghai Municipal Government 18JC1410800 and National Natural Science Foundation of China 51690151. This research used resources of the Advanced Photon Source, a US Department of Energy (DOE) Office of Science User Facility, operated for the DOE Office of Science by Argonne National Laboratory under contract number DE-AC02-06CH11357.

Author contributions M.H., S.W. and X.H. conceived the concept. X.H. supervised the project. M.H., S.W., Z.C. and Y.Z. conducted the experiments. J.S. and H.Z. helped with the WAXS and SAXS measurements. M.H., S.W. and X.H. wrote the manuscript. All authors contributed to the analysis and discussion of the data.

Competing interests The authors declare no competing interests.

Additional information

Supplementary information The online version contains supplementary material available at https://doi.org/10.1038/s41586-021-03212-z.

Correspondence and requests for materials should be addressed to X.H.

Peer review information *Nature* thanks Jiaxi Cui, Sylvain Deville and the other, anonymous, reviewer(s) for their contribution to the peer review of this work.

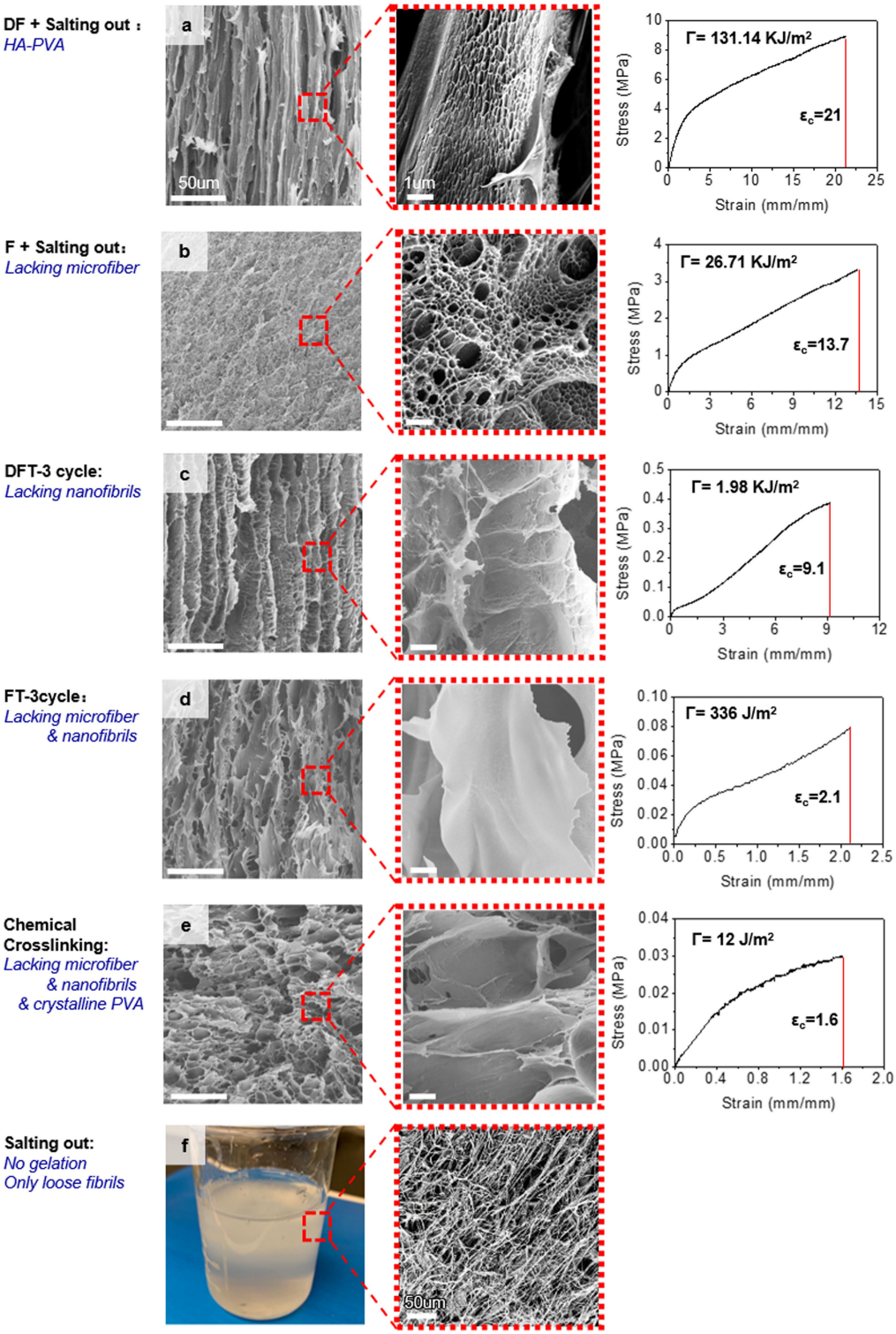

Extended Data Fig. 1 | Micro- and nanostructures and stress–strain curves of PVA hydrogels fabricated by different methods and their corresponding fracture energies and critical strains. a, 'DF + Salting out' denotes a hydrogel prepared by directional freezing of a 5% PVA solution and salting out in 1.5 M sodium citrate solution for 24 h. **b**, 'F + Salting out' represents a hydrogel prepared by non-directional freezing of a 5% PVA solution in the fridge and salting out in 1.5 M sodium citrate solution for 24 h. **c**, 'DFT-3 cycle' denotes a hydrogel prepared by directional freezing and thawing of a 5% PVA solution for three cycles. **d**, 'FT-3 cycle' indicates a hydrogel prepared by non-directional freezing in the fridge and thawing of a 5% PVA solution for three cycles. **e**, 'Chemical Crosslinking' represents a hydrogel prepared by mixing 0.5% glutaraldehyde and 0.5% hydrochloric acid into a 5% PVA solution for gelation. **f**, Salting out resulted in non-gelation. Only weak globules of loose and random nanofibrils were made by directly adding a 1.5 M sodium citrate solution into a 5% PVA solution. Panels **a**–**c** are the same as Fig. 3a–c.

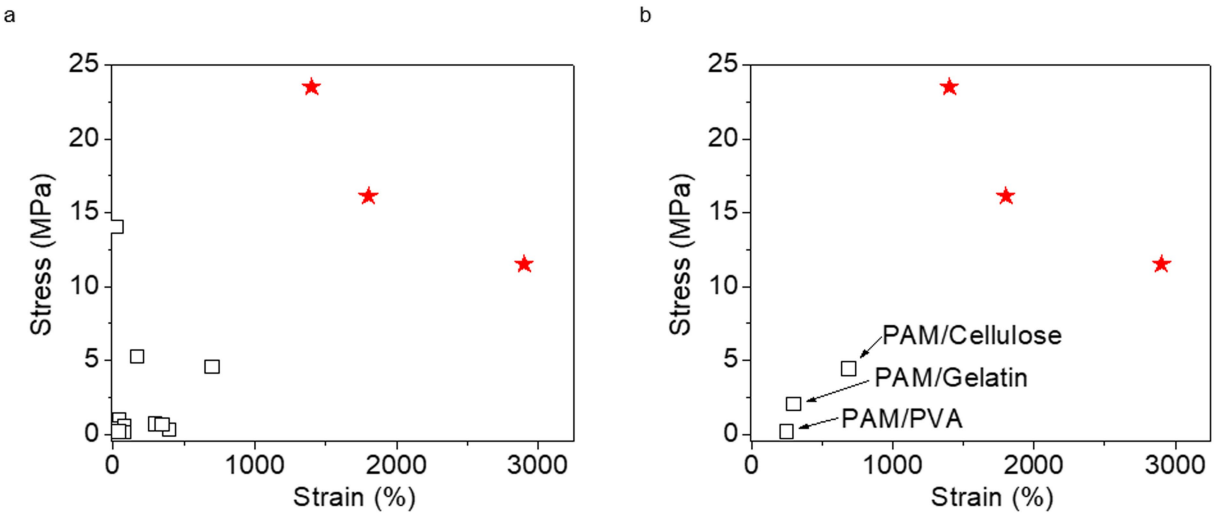

Extended Data Fig. 2 | Mechanical properties of HA-PVA hydrogel compared to those of PVA hydrogels prepared by ice-templating alone or salting out alone. a, **b**, The HA-PVA hydrogels are shown as red stars, and black squares correspond to the ice-templated PVA hydrogels (**a**) and the salting out PVA hydrogels (**b**). The data used are summarized in Supplementary Tables 1, 2.

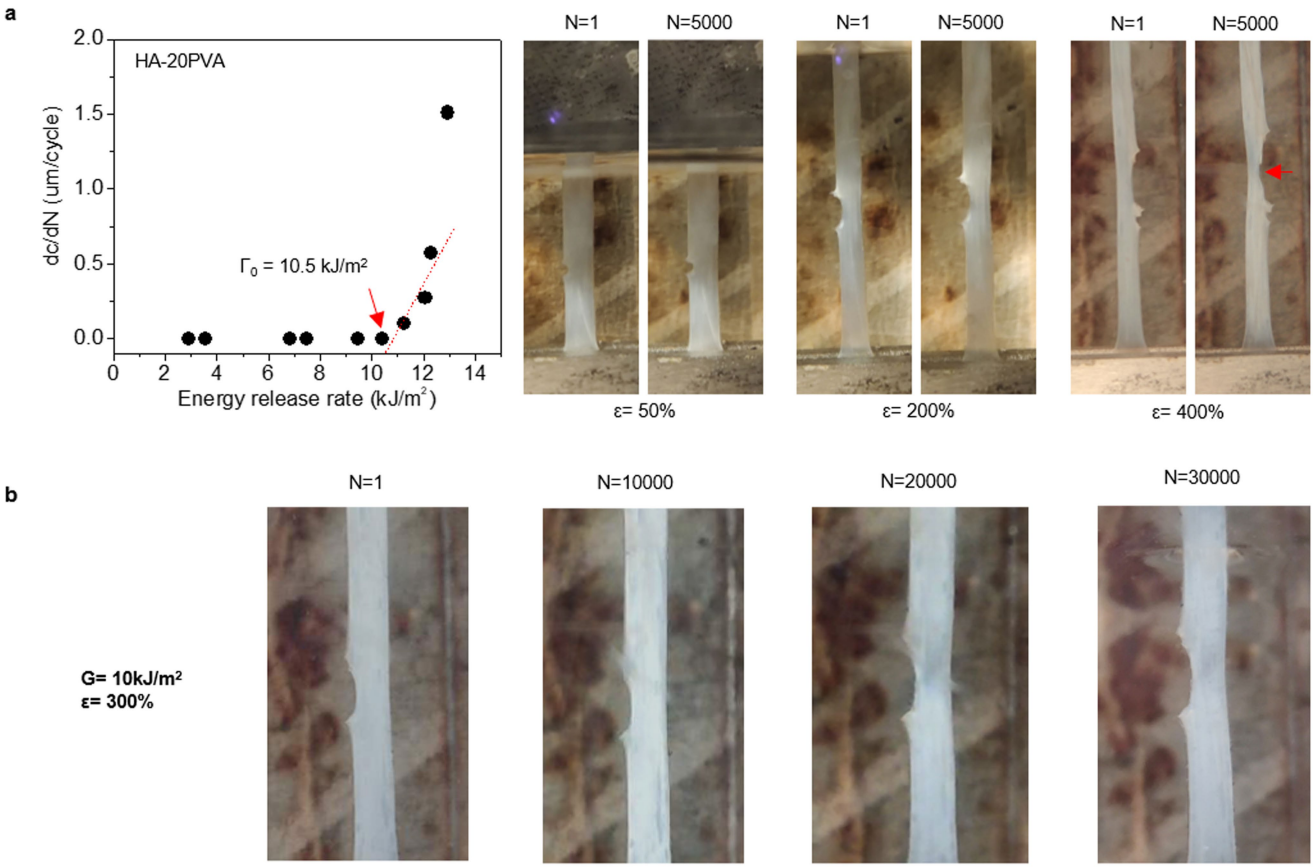

Extended Data Fig. 3 | Fatigue test of HA-20PVA hydrogels. a, Fatigue threshold of HA-20PVA. When loading above the threshold energy release rate ($\varepsilon = 400\%$), the crack propagates slowly. *N*, number of cycles. **b**, Validation of fatigue threshold with an energy release rate slightly lower than the fatigue threshold. No crack propagation or failure was observed for 30,000 loading cycles.

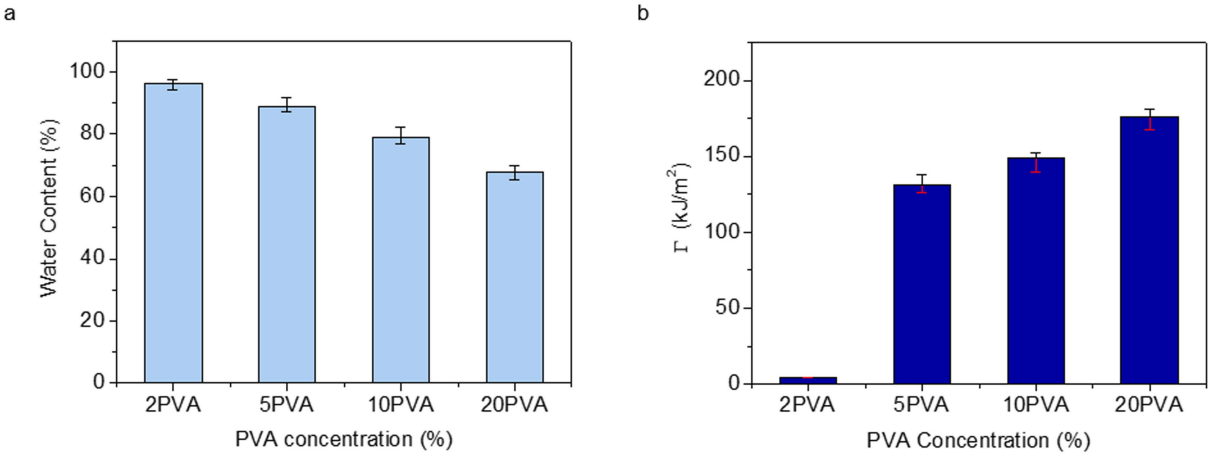

Extended Data Fig. 4 | Water content and fracture energy of the HA-PVA hydrogels. a, Water content of HA-*x*PVA hydrogels for $x = 2, 5, 10$ and 20. The error bars (1 s.d. from five measured samples) were obtained from five measured samples with standard deviations of 1.72%, 2.29%, 2.69% and 2.43% for $x = 2, 5, 10$ and 20, respectively. **b**, Fracture energy of HA-*x*PVA hydrogels, $x = 2, 5, 10$ and 20, measured by pure shear tests. The error bars (1 s.d. from five measured samples) were obtained from five measured samples with standard deviations of 0.16, 4.83, 5.44 and 5.62 kJ m^{-2} for $x = 2, 5, 10$ and 20, respectively.

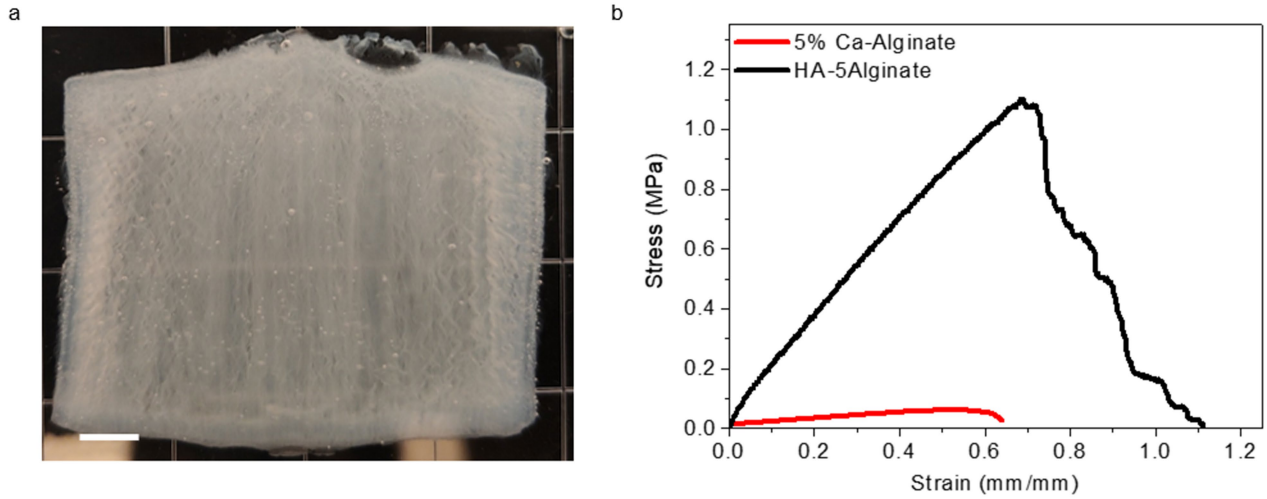

Extended Data Fig. 5 | HA-alginate hydrogels compared with calcium-alginate hydrogels. a, Photograph of HA-5alginate hydrogel. **b**, Tensile stress–strain curve of a HA-5alginate hydrogel compared to that of a regular calcium-alginate hydrogel. Scale bar, 5 mm.